Response to Referee #1

Thank you for carefully reading the manuscript and providing useful suggestions to improve the paper. The replies to the referee comments are given below. The referee comments are highlighted in blue with our responses in black. Some comments concerning similar issues are grouped together. The sentences in the manuscript are between the quotation marks, with the modifications in the revised manuscript in red.

The manuscript presents a Canadian biomass burning event measured by a multiwavelength Raman lidar (PollyXT) and a Vaisala CL51 ceilometer in Finland. The aerosol backscatter coefficients are converted to smoke mass concentration following the methodologies in literature. Comparison with model from MERRA-2 are shown as well.

I suggest the publication of this manuscript after addressing all the points raised by reviewers.

Please see below some suggestions and comments:

Pp 6, l 163-165: comment on the uncertainty of the water vapor absorption profiles used for the correction in the ceilometer backscatter profiles

Thank you for the comments. We have added descriptions about the water vapor corrections in section 2.3 in the revised version:

"

Wiegner and Gasteiger (2015) state that the annual variability of pressure and temperature has no significant influence on the water vapor absorption cross-sections. It is possible to use the tabulated mean absorption cross-section to calculate an approximative water vapor transmission with a high accuracy (the inherent error of the squared water vapor transmissions is <0.3 %; more details are given in section 4 in Wiegner and Gasteiger, 2015).

"

Fig. 1 Please add uncertainties to profiles. Also, mention the method you use to compute it.

We have added the uncertainty related to the wrong assumptions of the central wavelength when applying the water vapor correction in Fig.1. We also added the uncertainties in backscatter coefficients of the analytical solution in Fig.1. Further, we have added more description on the uncertainty study about forward and backward method in the revise version.

"

The uncertainties range due to wrong assumptions of $\lambda_0 \pm 2$ nm is given by the horizontal lines in Fig. 1. The uncertainties in backscatter coefficients of the analytical solution were also shown by dashed lines. As the water vapor contribution cannot be neglected at Kuopio during summer, the water vapor corrections have been applied to CL51 data in this study.

The retrieval methods for deriving the backscatter coefficient from ceilometers are quite mature (Wiegner et al., 2014; Wiegner and Geiß, 2012). Under favourable conditions, a relative error of the backscatter coefficient on the order of 10 % seems feasible with a careful calibration by applying the forward integration. On the contrary, significant temporal averaging of ceilometer data is required for performing a Rayleigh calibration, as the detection of molecular signals is intrinsically very difficult. Binietoglou et al. (2011) propose a two-step approach, resulting promising agreement comparing to their lidar PEARL (Potenza EARLINET Raman lidar). The uncertainty of the backscatter coefficient could be in the range of 20–30 % using the backward integration. The advantage of the forward algorithm is that calibration is required only occasionally, and it is not affected by the low SNR in the upper troposphere. However, the accuracy in deriving extinction coefficients is limited due to the unknown LR at 910 or 1064 nm and its uncertainties. In particular the presence of multi-layered aerosol distributions (with different aerosol types) may introduce more uncertainties. In addition, the uncertainty due to the neglecting the water vapor increased with the distance from the chosen reference height. In this study, we applied the Klett method (Wiegner et al., 2014) by defining the reference height as close as to the layer of interest, so that the error propagation (due to uncertainties of LR and water vapor transmission) would be minimized for that layer.

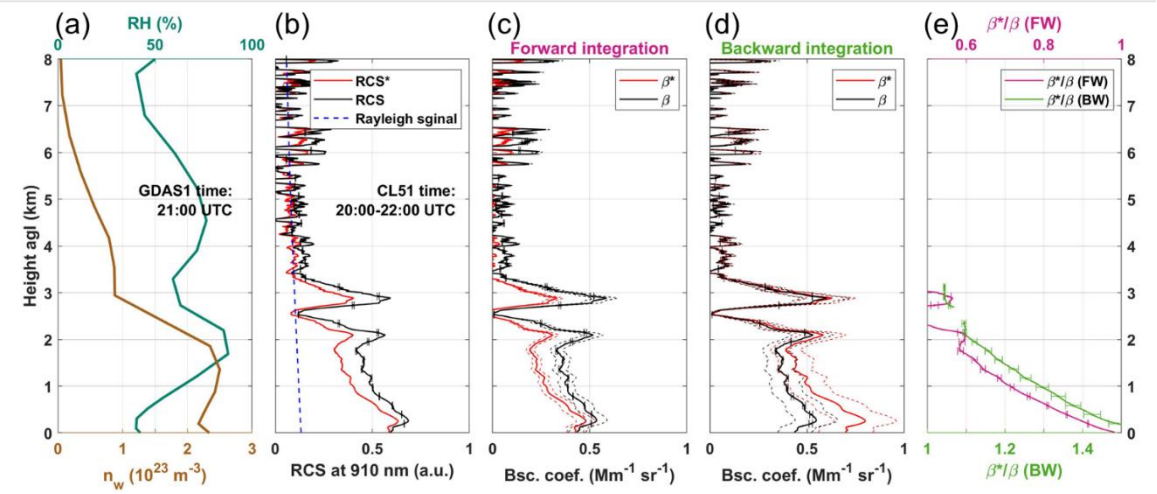

Figure 1. Example of water vapor corrections on 2 h averaged ceilometer data on 5 June 2019 (20:00–22:00 UTC). (a) Relative humidity (RH, teal) and water vapor number density (n_w, brown) from GDAS1 data at 21:00 UTC. (b) Range-corrected signal at 910 nm, without (RCS*, red) or with (RCS, black) water vapor correction, and the hypothetical Rayleigh-signal at 910 nm (dashed blue). (c) Retrieved particle backscatter coefficients: β* without (red) and β with (black) water vapor correction, using forward (FW) integration Klett solution. (d) Same as (c) but application of the backward (BW) integration. (e) Ratio of the retrieved β* and β, when using forward integration (magenta), or backward integration (green). The horizontal lines illustrate the uncertainties range due to wrong assumptions of the central wavelength $\lambda_0 \pm 2$ nm. The uncertainties in backscatter coefficients of the analytical solution were shown by dashed lines.

”

Pp 6, l 181: please add uncertainty for LR

We have added the uncertainty in the revised version as:

“

A value of 82 sr for LR, as measured at 1064 nm (82 ± 22 sr in Haarig et al., 2018), was assumed as being appropriate for use at 910 nm in this study.

”

Pp 6, l 192: please comment on the existence of the pollen. How do you know is pollen? Did you measure / estimate it? I guess it is typical to find pollen in June.

Thank you for the suggestion. We had in situ pollen measurements during the period. And you are right, June is a typical time of pine pollen for our site. This information was added in section 3 of the revised version:

“

Our in situ pollen measurements (more information about pollen instruments can be found in Bohlmann et al., 2021) shows high pine pollen loading (highest 2 h pollen concentrations were ~ 3000 m^{-3} on 5 June and ~ 7000 m^{-3} on 6 June). Although also of interest, the analysis of the pollen layer is out of the scope of this paper.

”

Pp 7, l 219-220: spatial resolution remains at 7.5m? Later you mention 11 bins sliding average for lidar and 7 bins for ceilometer. Please clarify.

Pp 9, l 274-275. For 11 bins gliding average over lidar profiles you obtain 82.5 m effective resolution. For the ceilometer, you obtain 70 m resolution. I was expecting more smoothing over ceilometer as it is much noisier. Please comment your choices.

Thank you for the suggestion. We have clarified this in the revised version.
In section 2.2 (Polly^{XT} lidar) we added:

“

The initial spatial and time resolution is 7.5 m and 30 s, respectively. The laser beams are tilted to an off-zenith angle of 5º to avoid specular reflections from horizontally aligned ice crystals. For the calculation of optical properties in this study, the profiles were temporally averaged in 2 h intervals, and smoothed with a vertical gliding averaging window length of 11 bins (a vertical range of ~ 82 m).

”

In section 2.3 (Ceilometer and data processing) we added:

“

The signal-to-noise ratio (SNR) for raw CL51 backscatter signals above the boundary layers is weak, hence some temporal averaging and vertical smoothing were required when performing further analysis. In this study, CL51 signals were smoothed with a vertical gliding averaging window length of 7 bins (a vertical range of ~ 70 m). The profiles were temporally averaged in 10 min intervals for the time–height cross section quick look, and in 2 h intervals to calculate the optical properties.

”

We have also recalled this information in section 3.1 (Optical properties) for the clarity:

“

Layer-mean values of optical properties of the SPoI were derived and are given in Table . Two-hour time-averaged, and vertical smoothed (with a smoothing window of ~ 82 m) lidar profiles were used in order to increase SNR.

”

In our data processing program, we used odd number of bins as the sliding window, and we select 11 bins for PollyXT and 7 bins for ceilometer, so that they are more or less the similar vertical smoothing (we can also choose 9 bins for ceilometer). As we mainly consider the layer mean values, the vertical smoothing doesn’t have significant impacts on the results. We think 7 bins are good enough for our smoke layer study, as the CL51 has enough power.

Pp 7, l 195-199: please comment on the choices for AE. Why did you choose the ratios 500/870 and 380/500? Is it the later chosen for comparison with lidar’s EAE (e.g. Muller et al., 2013; Nicolae et al., 2019). When you refer to fine particles do you refer to those smaller than 1 um?

Pp 8, l 227-231: EAE of 1.4 is suggested as a delimitation from fresh and aged smoke along with LR532 > LR355 (Nicolae et al., 2013). Higher values of EAE correspond to smaller effective radius (e.g., Muller et al., 2005). Please clarify how you consider the range of fine particles. If you consider fine particles those smaller than 1 um (as for photometer), then we measure fine mode particles with the lidar most of the time. On the other hand, one can consider 500 nm as the delimitation between fine-mode and coarse-mode (e.g., Muller et al. 2016). Mamouri and Ansmann refer to fine dust if the particle’s radius is < 500 nm. Please comment on the value of EAE derived from lidar (1.4) and discuss the relationship with AE from photometer for 380/500 assuming the value is similar with that corresponding to 355/532. As seen in Fig. 3, AE for 5th of June is around 0.8-1.05. I would have expected closer values for EAE and AE.

Thank you for the comment. We have changed this figure from AE 500/870 to AE 500/1020, as follows. These selected 3 wavelengths (380, 500, and 1020) in the revised version are more close to our PollyXT lidar wavelengths (355, 532, and 1064). We found that the values of AE 500/870 and AE 500/1020 were quite similar. Here, we used the AEROENT level 2.0 aerosol spectral deconvolution algorithm (SDA) products, which yield fine (sub-micron) and coarse (super-micron) aerosol optical depths at a standard wavelength of 500 nm. Related information has been added in the revised version.

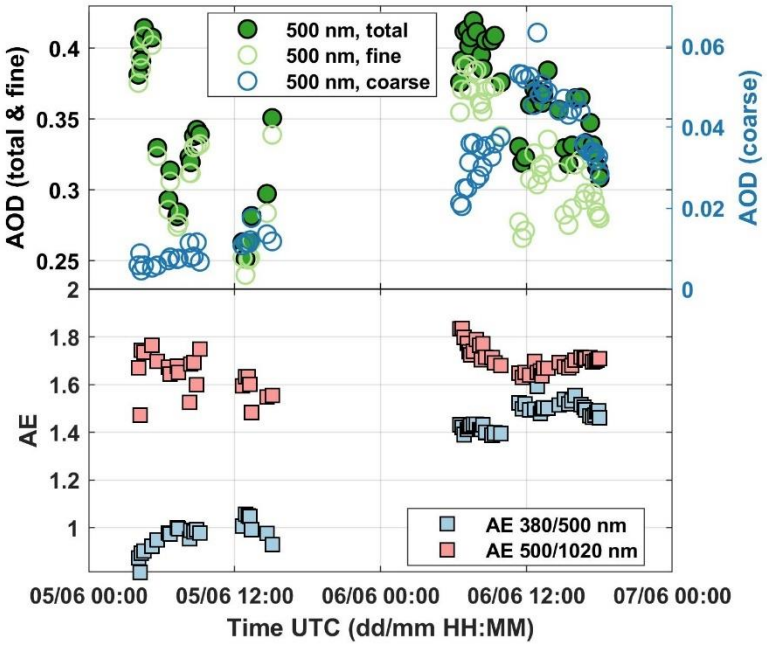

Figure 3. AERONET sun-photometer observations (in Kuopio station, on 5 and 6 June 2019, http://aeronet.gsfc.nasa.gov, last access: 3 May 2021) of (top) 500 nm aerosol optical depth (level 2.0 data) and (bottom) Ångström exponents (AE) computed from the optical depths measured at 380, 500, and 1020 nm. The fine-mode-related (for particle with diameters < 1μm) and coarse-mode-related aerosol optical depth (diameters > 1μm) are shown in addition (top, level 2.0 aerosol spectral deconvolution algorithm (SDA) products).

We can compare these sun-photometer AE with lidar's EAE. However, note that the sun-photometer AE is for the total atmospheric column (as we mentioned in section 2.1), whereas lidar's EAE in Table 1 is only for the smoke layer. On 5th, there were cirrus presence (this is also the reason why there was no AERONET inversion product available on 5th) above the smoke layer, and pollen or other aerosols presence in the PBL; please find following figure of PollyXT RCS at 1064 nm (in the manuscript, the y-axis of Fig.2a was cut at 8 km). Also, the lidar's EAE was only available for night-time (between 5th and 6th), but sun-photometer AE was for daytime. If we interpolate the sun-photometer AE of 5th and 6th, a better agreement can be found for lidar's EAE. We have added descriptions for the clarity in the revised version.

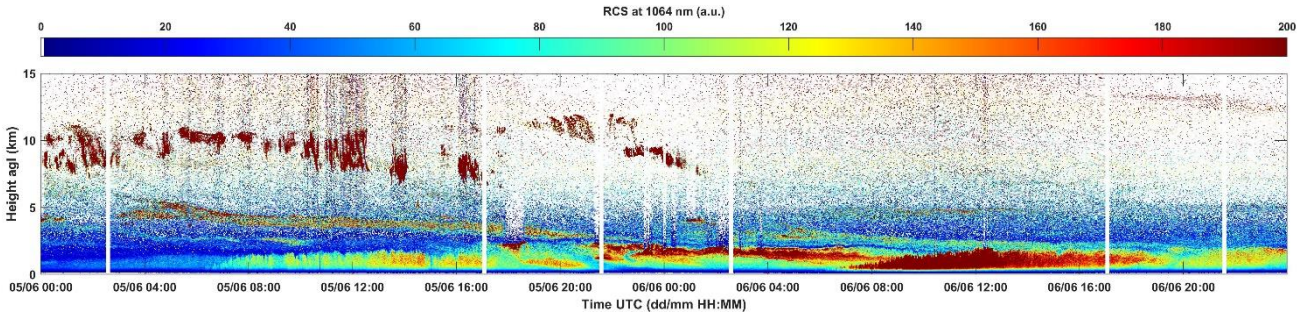

Thank you for the suggestion about "EAE of 1.4 is suggested as a delimitation from fresh and aged smoke", we have added such information in the revise version.

We haven't performed the microphysical analysis to estimate the effective radius, but we have added descriptions about possible effective radius value (0.23 μm), based on figure 6 in Muller et al. 2005. We have also added one column of the effective radius values from literature in Table 1 (please check our reply to your later comment).

Please see our modifications in the revised version about previous points as follows:
In section 3.1:
"

Nonetheless, the wavelength dependence of the extinction coefficient for the 355–532 nm spectral range is much weaker, with an extinction-related Ångström exponent (EAE) of ~ 1.4. Nicolae et al. (2013) state that the EAE can be used for identifying the evolution of ageing processes of biomass burning aerosol, as it decreased from 2 for fresh to ~ 1.4–0.5 for ages biomass burning aerosols. The microphysical analysis was not performed in this study; yet the measured EAE would be related to the effective radius of ~ 0.23 µm, when considering the relationship between EAE and effective radius of forest fires smoke reported by Müller et al., (2005) (c.f., Fig. 6 in that paper). This estimated effective radius value is consistent with those of aged smoke aerosols reported in literature (Table 1). The AERONET sun-photometer Ångström exponent at 380–500 nm on 5 June showed lower values than lidar EAE at 355–532 nm; possible cirrus contamination could partly explain as sun-photometer data are for the total atmospheric column. Note that lidar's EAE was only available for night-time (between 5th and 6th).

"

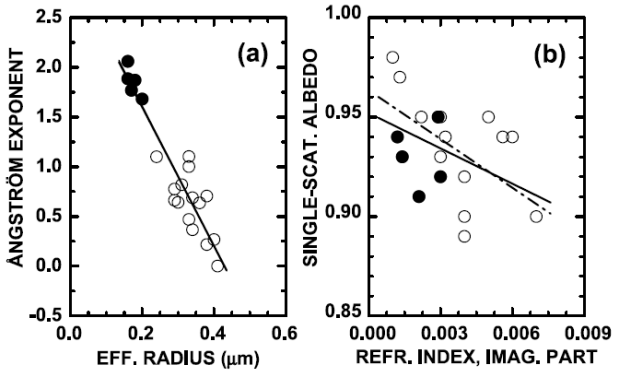

Figure 6. Correlation plot of (a) Ångström exponent versus effective radius and (b) single-scattering albedo versus imaginary part of the complex refractive index. Open circles denote cases of forest fire smoke. Solid circles describe the case of anthropogenic pollution. Regression lines denote best linear fit. In the case of Figure 6b, fit is shown under consideration of all data points (solid line) and if only data points representing forest fire smoke are considered (dash-dotted line).

Figure 6 from Muller et al. 2005.

Regarding the range of fine particles, we consider fine particles as for the photometer. Thank you for pointing it out, we made modifications to clarify it in the revised version.
In section 2.1 for AERONET data descriptions, we added:

"

The volume particle size distribution was retrieved in the range of radius of 0.05–15 µm; the minimum within the size interval from 0.439–0.992 µm was used as a separation point between fine and coarse mode particles.

"

in the new section 3.2.2 when we used AERONET fine mode data, we added:

"

From the size distribution, the separation points between fine and coarse mode particles were found as ~ 0.576 µm (the size classes 1–10 were considered for fine-mode aerosols).

"

in the new section 3.3 when we applied the separation method, we added:

"

The POLIPHON (Polarization lidar photometer networking) method (Mamouri and Ansmann, 2014, 2017) was applied to separate fine dust (particles with radius < 500 nm) and biomass burning aerosols for the SPoI.

"

Pp 8, l 241-243: PDR@532 > 5% are observed in literature for aged smoke. Please check the literature review by Adam et al. 2020 (see Supplement).

Table 1. You can add values for BAE from Ancellet by converting CR to BAE. Also, you can add the case of pure BB. More values from literature are given by Adam et al. 2020, Supplement.

Thank you for the suggestion. We have enriched the information for Table 1. We have removed the case from Muller et al. 2007, as the source region was Siberia, but added other references (with source regions for Canada or North America) as shown in red in the table. We have also added one column of the effective radius values.
We have converted CR values in Ancellet et al. 2016 to BAE as shown in table below.
"

Table 1. Optical properties (lidar ratio, particle linear depolarization ratios-PDR, backscatter- or extinction-related Ångström exponent-BAE or EAE) of biomass burning aerosols. Layer-mean values of the SPoI (Smoke Plume of Interest) and the standard deviations are given. Optical properties and the effective radius (R_{eff}) found in literature of aged forest fire smoke aerosols observed in the troposphere are also given for comparisons. The source regions of these smoke aerosols are all Canada and/or North America ~~Siberia~~.

	Lidar ratio (sr)			PDR (%)		Ångström exponent			R_{eff} (µm)
	355	532	1064	355	532	EAE 355/532	BAE 355/532	BAE 532/1064	
This study	47 ± 5	71 ± 5	-	8 ± 2	5 ± 1	1.4 ± 0.2	2.5 ± 0.2	2.2 ± 0.3	-
Ancellet et al. (2016)	-	60 ± 20	-	-	<5	-	-	1.3–2.3	-
Ancellet et al. (2016)*	59 ± 5	60 ± 5	-	5–8	5–10	-	2.6	1.0–1.3	-
Gross et al. (2013)	-	69 ± 17	-	-	7 ± 2	-	-	2.2 ± 0.4	-
Haarig et al. (2018)	46 ± 6	67 ± 4	82 ± 22	2 ± 4	3 ± 2	0.9 ± 0.5	2.1 ± 0.6	0.8 ± 0.3	0.17 ± 0.06
Janicka et al. (2017)	60 ± 20	100 ± 30	-	1–5	2–4	0.3–1.7	1.7–2.1	1.3–1.8	0.31–0.36
Muller et al. (2005)	21–49	26–64	-	-	-	0.0–1.1	-	-	0.24–0.4
Ortiz-Amezcua et al. (2017)	23–34	47–58	-	-	2–8	0.2–1.0	1.2–1.9	-	0.21–0.34
Wandinger et al. (2002) and Fiebig et al. (2002)	40–70	40–80	-	-	6–11	-	-	-	0.27 ± 0.04

* Biomass burning mixing with a small amount of dust.
"

We agree that the conclusion of "PDR were slightly higher than the values given in the literature" is too speculative, we have removed related sentences and made modifications in the revised version:
"

The smoke particles caused slightly enhanced particle linear depolarization ratios (PDR) at 355 nm (532 nm) with a mean value of 0.08 ± 0.02 (0.05 ± 0.01) in the smoke layer, suggesting the presence of partly coated soot particles or particles that have mixed with a small amount of dust or other non-spherical aerosol type. The layer-mean PDR at 355 nm (532 nm) decreased during the day, from ~ 0.11 (0.06) in the morning to ~ 0.05 (0.04) in the evening. The decrease of the PDR with time could be linked to the particle aging and related changed in the smoke particle shape properties, as stated by Baars et al. (2019). The relative humidity (RH) profiles from GDAS1 data showed low values in the lower atmosphere (<60 % below 6 km) before 15h UTC, and even lower RH (<40 %) at the SPoI altitude. RH slightly increased in the evening. The signal in the 407 nm Raman-shifted channel was used to determine the water vapor mixing ratio profile during night-time, showing that the layer-mean RH changed from ~ 27 % at 19 h to ~ 38 % at 23 h, which was associated with the advection of a moister air mass with a water vapor mixing ratio close to 1–3 g kg^{-1}. The smoke particles were dry, and then captured water vapor in the atmosphere during the evening. The decreasing temperature and increasing RH also increase the probability that smoke particles become glassy. The depolarization ratios of aged biomass burning aerosols (originating from Canada and/or North America) reported in the literature (Table 1) range from 0.01 to 0.11 (0.01 to 0.08) at 532 nm (355 nm). More information of the aged smoke from other regions can be found in the literature review by Adam et al. (2020, see the Supplement).

"

Pp 9, l 278. You mention a maximum value of 45 ug/m3. Please mention to which profile you refer to (355, 532, 910) and the time interval. Also, please add comments on morning and night values as you mention in abstract and summary. Please add the profile at 1064nm as this one compares better with 910nm (closer wavelengths).

Pp 11, l 319: please add numerical values when discussing 'large discrepancies' or good agreements between mass concentrations estimated from 355, 532 and 910. A simple way is to compare the mean value in the layer from each profile. Then you can mention the minimum and maximum differences between profiles.

Pp 12, 355: as said, add few comments in the text about those 30 and 20 ug/m3 values in the morning and in night. Nothing is specified in the main text. Mention the time it was observed and the profiles (e.g., 355, 532, 910). When looking at Fig. 6, I can see values of mass concentration around 30 ug/m3 in 532 profile at 06:00 and 09:00. However, I can see also values at 30 ug/m3 at 21:00. I don't know where 20 ug/m3 is observed.

Pp 12, l 354: please comment quantitatively on 'good agreement'; see above. Also, comment on the agreement between ceilometer and the retrieval of mass concentration starting from 1064 backscatter profile (first, add this profile).

Fig. 6. Please add uncertainties to profiles.

Thank you for the very useful suggestions.

We have added the 1064 nm profiles for additional information. The factor at 1064 nm were added in Table 2 in the revised version:

"

Table 2. Parameters required for the mass concentration retrieval using two methods. The smoke mass density (ρ) and lidar ratio at 532 nm are common parameters required for both methods #1 and #2.

	Parameter	Wavelength	Value	References
Common	Smoke mass density (g cm^{-3})	-	1.3	Ansmann et al. (2021)
	Lidar ratio (sr)	532	71 ± 5	This study
Method #1	Smoke volume-to-extinction conversion factor c_v (10^{-6} m)	532	0.13 ± 0.01	Ansmann et al. (2021)
	Backscatter-related Ångström exponent	355/532	2.5 ± 0.2	This study
		1064/532	2.2 ± 0.3	
		910/532	1.8 ± 0.2	
Method #2	Lidar ratio (sr)	355	47 ± 5	This study
		1064	82 ± 22	Haarig et al. (2018)
		910	82 ± 22*	Haarig et al. (2018)
	Fine-mode volume-to-extinction conversion factor c_v (10^{-6} m)	355	0.100 ± 0.002	This study
		532	0.211 ± 0.003	(Possible pollution contamination)
		910	0.620 ± 0.002	
		1064	0.902 ± 0.004	

* LR values measured at 1064 nm are used for LR at 910 nm.

"

The mass profiles estimated from backscatter coefficients at 1064 nm (in red color) have been added in the revised figures as well.

We have added uncertainties on the backscatter coefficients (Fig.5 a,b). But it will be too messy if we add such information on Fig.5c due to the large uncertainties on the mass concentration. Nevertheless, we have emphasized this in the figure caption.

In addition, we have added a new sub-figure (Fig.5d) to show the difference on the estimated mass concentrations as follows:

"

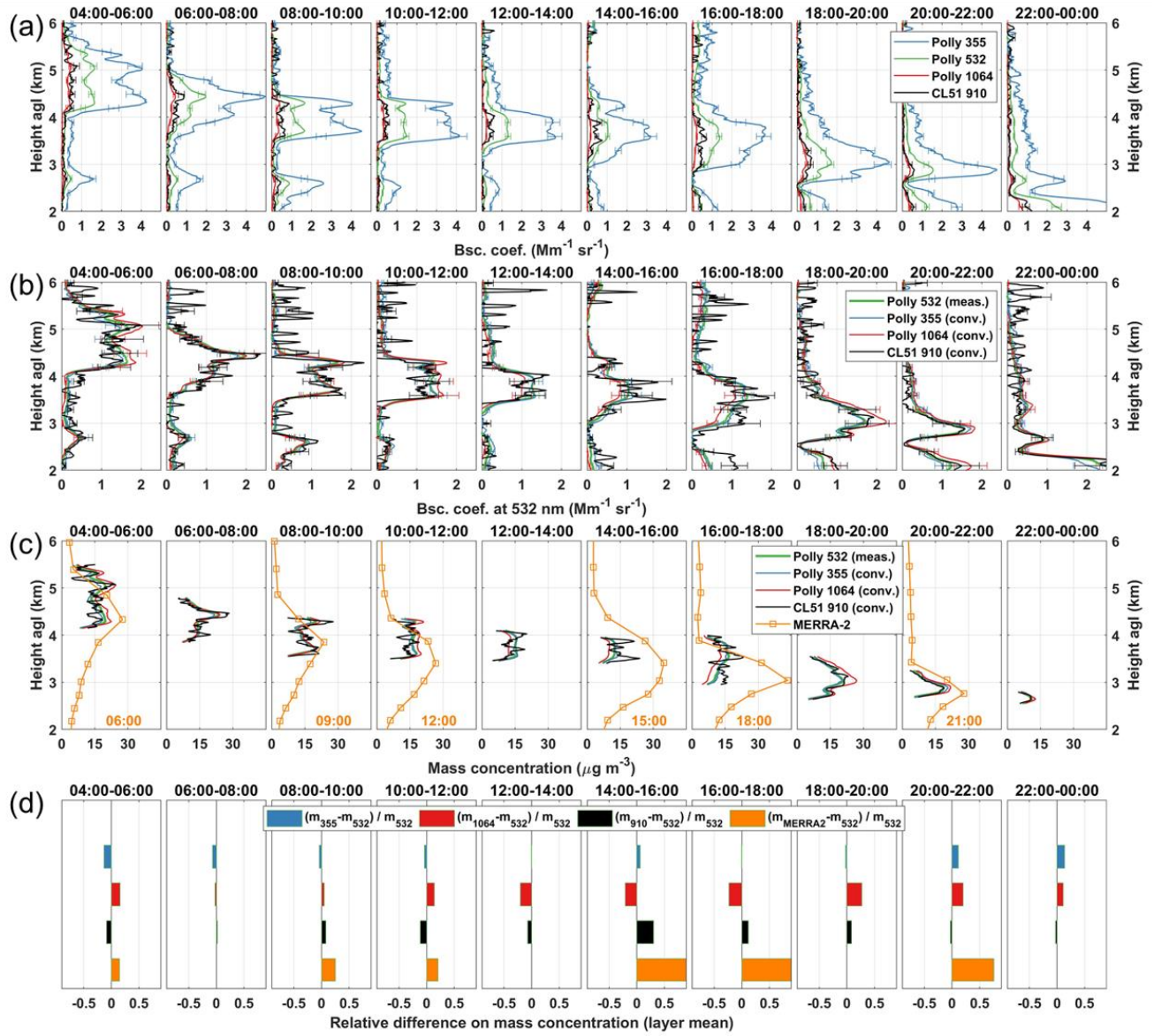

Figure 6. (a) Lidar-derived backscatter coefficients (BSC) at 355 (blue), 532 (green), and 1064 nm (red) from Polly^{XT}, and at 910 nm (black) from CL51. (b) BSCs at 532 nm: measured at 532 nm (meas.), or converted (conv.) from measured BSCs at other wavelengths. (c) Estimated mass concentration profiles for the SPoI (Smoke Plume of Interest) using BSCs in (b), based on parameters in Table 2-method #1. Mass concentrations from MERRA-2 model are also shown in orange colour with corresponding time given on the bottom right of each panel. (d) Relative differences on the mass concentrations (denoted as *m*) estimated from measured/converted BSCs, and of MERRA-2 model, using the one from measured BSC at 532 nm as the reference. 2 h time-averaged lidar profiles are used, with the time slot (UTC) on 5 June 2019 given on top of each panel. The horizontal lines (in a, b) illustrate the uncertainties range. The uncertainties in mass concentrations (in c) are discussed in Sect. 3.2.1.

”

Concerning the quantitative description on ‘mass concentration value’, ‘good agreement’ or ‘large discrepancies’, we have carefully checked the manuscript and made the modifications in the revised version:
In section 3.2.1 “Method #1: based on BAE & the conversion factor from literature”:
“

The peak value of the mass concentrations was found at 6–8h UTC, of ~ 23.5 (27.5) μg m^{-3} estimated from the backscatter coefficients at 532 nm (910 nm). If we take the mass concentration estimated from the BSC at 532 nm as the reference, good agreements are found between the mass concentrations estimated from BSCs at different wavelengths (Fig. 5 d). The mean values of the relative differences were around 8 %, 12 %, and 18 % for the estimations from BSCs at 355, 910 and 1064 nm, respectively. Comparing 532 and 355 nm mass estimates, better agreements were found during daytime (8–20h UTC), with a difference <6 %. Nonetheless, considering

532 and 910 nm estimates, the best agreements were found at 6–8 and 20–24h UTC, with a difference <3 %, whereas the worst agreement of ~ 30 % was found at 14–16h UTC. Larger differences between 910 and 1064 nm estimates were found, with a mean relative difference of ~ 28 %, and a highest value of ~ 64 % at 14–16h UTC.

”

In section 3.2.2 “Method #2: BSC at each wavelength & conversion factors from site”:

“

The peak value of the mass concentrations estimated from the BSCs at 532 nm reached ~ 38 µg m^{-3} at 6–8h UTC, higher than the one estimated from method #1 because of the bigger conversion factor. The relative differences on the mass concentrations estimated from the BSCs at different wavelengths were analysed (Fig. 7 b). Similarly, we take the mass concentration estimated from the BSCs at 532 nm (which is the wavelength most often used in earlier studies) as the reference, and found an underestimate when using BSCs at 355 nm, with a mean bias of ~ 15 %, and a peak bias of ~ 25 % at 4–6h UTC; the best agreement was found for night-time measurements (20–24 h UTC) with a bias <5 %. Nevertheless, an overestimate was found for the mass concentration estimated from the BSCs at 910 nm, with a mean bias of ~ 36 %, a peak bias of ~ 68 % at 14–16h UTC, and a minimum bias of ~ 14 % at 10–12h UTC. The overestimate for CL51-derived mass concentrations could be due to an overestimate of LR at 910 nm, since we used LR at 1064 nm in the calculations. In addition, big differences (with a mean value of ~ 42 %) were found between the CL51-derived mass concentrations and the ones estimated from the Polly^{XT}-derived BSCs at 1064 nm; highest discrepancy were found of ~ 95 % at 14–16h and ~ 75 % at 16–18h UTC, whereas better agreements were found at 4–6h, 10–12h, and 18–24h, with bias <7 %.

”

In section 3.3 “Comparison with MERRA-2 model - wildfire smoke and dust aerosol mixture”:

“

In this section, the MERRA-2 mass concentrations were compared with the mass concentrations estimated from the Polly^{XT} backscatter coefficients at 532 nm (from method #1-Fig. 5 c, and method #2-Fig. 7 a). Note that the main difference on Polly^{XT}-estimated mass concentrations from two methods are due to the different conversion factor values (Table 2), thus the mass concentrations estimated from BSCs at 532 nm using method #1 are ~ 40 % lower than method #2. When the Polly^{XT} estimates from method #1 were used as the reference, good consistencies were found in the morning (at 6h, 9h, and 12h UTC), with overestimations (<30 %) of MERRA-2 mass concentrations; whereas large discrepancies were found in the afternoon, with high overestimations of ~ 160 % at 15h UTC and ~ 90 % at 18h UTC. If the Polly^{XT} estimates from method #2 were used as the reference, good consistencies were also found in the morning (at 6h, 9h, and 12h UTC), but with underestimations (<30 %); and a large overestimation of ~ 63 % was found at 15h UTC. At 15h UTC, the MERRA-2 simulated dust mass concentration fraction is more than half of the MERRA-2 simulated total mass concentration. It is good to keep in mind that both observations and simulations have significant uncertainties. The presence of cirrus cloud in the upper atmosphere during the day may also have some impacts on MODIS AOD, which is assimilated by the MERRA-2 model.

”

Pp 10, l 300. From the text I understand that the fine dust comes from N America. Please comment and justify the presence of dust. I would rather think about Saharan dust as the event described by Osborne et al. (2019). I guess the Hysplit did not show backtrajectories towards N Africa in your case. I saw that MERRA-2 shows a dust component.

Thank you for the comments. Using Hysplit, we found that the air mass comes from the N America not N Africa. We have checked the AIRS dust score (figure below), it shows that there was dust (inside the red circle in the figure) in N America on the day when the air mass passed by. We have added this information in the revised version for the clarity.

In section 2.1, we added:

“

The “Dust score” data provided by AIRS (Atmospheric InfraRed Sounder) were used to determine the occurrences of dust events (https://airs.jpl.nasa.gov, last access: 1 July 2021).

”

In section 3, we added:

“

The backward trajectory analysis was performed using the HYSPLIT model. The analysis shows that particles in the SPoI had travelled about seven days from the forest fire sources (MODIS, 2019) in western Canada to North Europe (Fig. 4). The AIRS dust score map (https://airs.jpl.nasa.gov/map/, last access: 1 July 2021) also showed some dust presence in North America on 30 May.

”

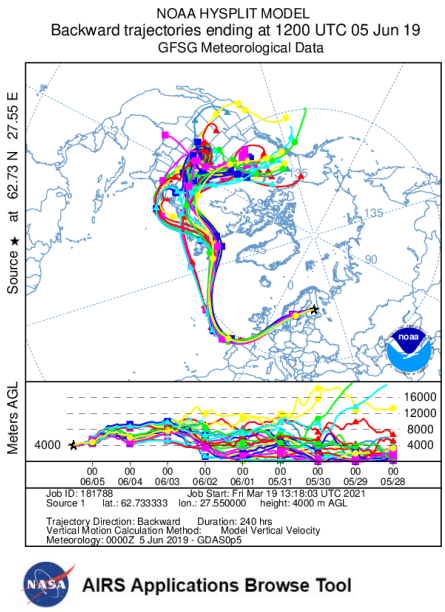

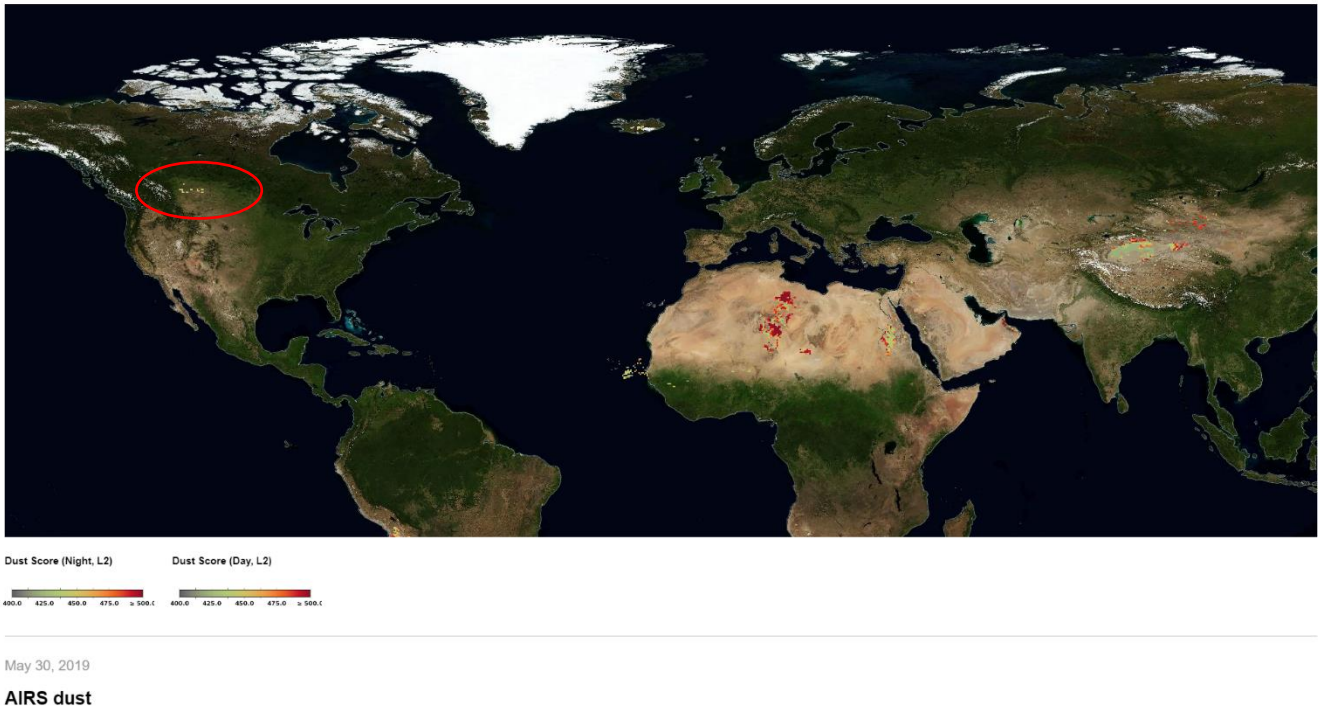

Pp 12, 357-359: taking into account the uncertainties in the retrieval of the mass concentration, the improvement by 4% using dust contribution seems not very relevant.

We agree, so we have removed the Fig.6c (of old version) as it shows only few information.
We performed this separation study in order to check how the inclusion of dust (as indicated by MERRA-2) would affect the mass concentration estimations. We found out that the inclusion of a dust mixture results in slightly

higher estimated mass concentration values, with a difference negligible considering the uncertainties. Thus, we conclude that lidar and ceilometer observations for mass retrievals can be used even without exact knowledge on the composition of the smoke plume in the troposphere.
We have clarified this in the revised version:
In section 3.3 “Comparison with MERRA-2 model - wildfire smoke and dust aerosol mixture”:
“

The mass concentrations from MERRA-2 model data are used for the comparison with the lidar retrievals. An interesting feature in the MERRA-2 simulation results is the presence of dust in the SPoI. The contribution of dust to the total AOD is very low (much lower than the carbon optical depth), indicating that the dust particles are in the fine mode. However, the dust contribution to the total mass concentration is non-negligible. Low values of lidar-derived depolarization ratio suggest no significant presence of non-spherical particles, but in principle, a small amount of dust could be mixed with the smoke. It is possible that there are biomass burning aerosols and fine dust aerosols in the SPoI, as only fine dust particles should be able to remain long enough in the atmosphere to be transported from North America to Kuopio. Furthermore, the air masses in SPoI passed by the area in North America where dust was present (shown by the AIRS data).

…

In order to check how the inclusion of dust (as indicated by MERRA-2) would affect the mass concentration estimations, we assume that there were wildfire smoke and fine dust aerosol mixture in the SPoI. The POLIPHON (Polarization lidar photometer networking) method (Mamouri and Ansmann, 2014, 2017) was applied to separate fine dust (particles with radius < 500 nm) and biomass burning aerosols for the SPoI.

…

For the example given in Fig. 8, the fine dust contributes ~ 13 % to the extinction in the SPoI, whereas its mass concentration contributes ~ 32 % (method #1) or ~ 23 % (method #2) to the total mass concentration. However, the derived total mass concentration considering a fine dust and smoke mixture is only ~ 18 % (method #1) or ~ 4 % (method #2) higher than one assuming smoke particles only. The inclusion of a dust mixture results in slightly higher estimated mass concentration values, with a difference negligible considering the uncertainties.
We have also performed POLIPHON considering coarse mode dust mixture; higher (~20–30 %) total mass concentrations were retrieved but still within the uncertainty range. The aged smoke aerosols may also introduce enhanced depolarization ratios. If we use a bigger value (e.g., 0.05) instead of 0.03 as the smoke depolarization ratio in POLIPHON, the dust impacts on the mass concentration estimations are even smaller. Hence, the mass estimations of the SPoI considering only smoke are good enough even if the plume contains small amount of dust.
Similar conclusion can also be applied to ceilometer observations. It is not possible to perform the aerosol separation using ceilometer data alone, as no depolarization information is available at this wavelength. For this instrument, only one aerosol type should always be assumed in the layer of interest, which then imparts an additional bias when estimating the mass concentration. However, we have shown in this section that ceilometer observations for mass retrievals can be used even without exact knowledge on the composition of the smoke plume in the troposphere.

”

Change units from um to ug.

The correction has been done.

Fig 5. Please add uncertainties to profiles.

We have removed this figure and also the text about in situ measurements in the revised version.

Fig. 7 please add uncertainties to profiles.

We have added the uncertainties.

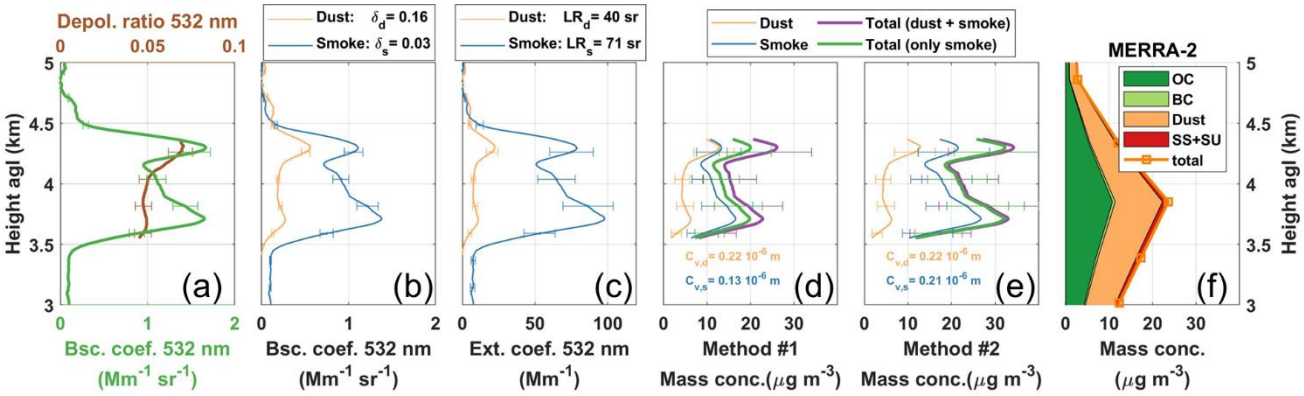

Figure 8. Lidar products obtained from Polly^{XT} measurements on 5 June 2019, 8–10h UTC (2h signal average). (a) Measured 532 nm total particle backscatter coefficient (green) and particle linear depolarization ratio (brown). (b) Particle backscatter coefficients (BSCs) for fine dust (orange) and smoke (blue) particles, obtained with the POLIPHON method. (c) Respective fine dust and smoke extinction coefficients (EXTs) obtained by multiplying the BSCs (in b) with the lidar ratios. (d,e) The fine dust (orange), smoke (blue) particle mass concentrations derived from the EXT profiles (in c), by using parameters in Table 4 for method #1 (d) and #2 (e). The total mass concentrations of fine dust and smoke mixture (purple), or of only smoke particles (green) are shown. (f) Mass concentrations of organic carbon (OC, dark green), black carbon (BC, light green), dust (orange), sea salt and sulphate (SS+SU, red) from MERRA-2 model, at 9h UTC on 5 June. The total mass concentration profile is also given by orange squares. The horizontal lines illustrate the uncertainties range.

References:

Adam et al., 2020 : https://acp.copernicus.org/articles/20/13905/2020/

Mamouri and Ansmann, 2017 : https://amt.copernicus.org/articles/10/3403/2017/

Muller et al., 2005 : https://agupubs.onlinelibrary.wiley.com/doi/full/10.1029/2004JD005756

Muller et al., 2013 : https://www.osapublishing.org/ao/fulltext.cfm?uri=ao-52-14-3178&id=253294

Muller et al., 2016 : https://amt.copernicus.org/articles/9/5007/2016/

Nicolae et al., 2013 : https://agupubs.onlinelibrary.wiley.com/doi/full/10.1002/jgrd.50324

Nicolae et al., 2019 : https://www.mdpi.com/2073-4433/10/9/482

Osborne et al., 2019 : https://acp.copernicus.org/articles/19/3557/2019/